Research Square

Preprints are preliminary reports that have not undergone peer review.
They should not be considered conclusive, used to inform clinical practice,
or referenced by the media as validated information.

# Eco-Friendly $In_xGa_{1-x}N$ Colloidal Quantum Dots for Light Emitting Diodes

**Yangpil Jang**
Ulsan National Institute of Science and Technology
**Yo-Han Suh**
Ulsan National Institute of Science and Technology
**Jongnam Park**
jnpark@unist.ac.kr

Ulsan National Institute of Science and Technology https://orcid.org/0000-0002-0954-0172

**Research Article**

**Keywords:** Metal nitride, Group III-V, Colloidal quantum dots, Eco-friendly, Quantum dot Light emitting diode

**Posted Date:** October 30th, 2026

**DOI:** https://doi.org/10.21203/rs.3.rs-11360456/v1

**License:** This work is licensed under a Creative Commons Attribution 4.0 International License.
Read Full License

# Abstract

We report the synthesis of emissive $In_xGa_{1-x}N$ colloidal quantum dots (CQDs) by using a hot-injection method and the demonstration of quantum dot light-emitting diodes (QLEDs) utilizing these CQDs. We successfully synthesized size- and composition-tunable $In_xGa_{1-x}N$ CQDs (x= 0 ~ 1) using the hot injection method and investigate the structural and optical properties of these CQDs as a function of the ratio of In to Ga. Through particle size control, green and blue emissive $In_xGa_{1-x}N$ CQDs were realized. The X-ray absorption fine structure (XAFS) results indicate that the crystal states of the $In_xGa_{1-x}N$ CQDs consist of multiphase states; multipeak photoluminescence (PL) resulted from these multiphase states. The multiple peaks correspond to the changes in the PL spectra due to variations in the metal fractions. Inverted structured QLEDs exhibited green electroluminescence (EL) emission and a maximum luminance of ~45 cd/$m^2$. These results indicate that $In_xGa_{1-x}N$ CQDs can serve as promising alternatives to conventional cadmium-containing CQDs in various optoelectronic applications, e.g., eco-friendly displays.


# Introduction

Colloidal quantum dots (CQDs) have attracted considerable attention as promising materials for use in various optoelectronic devices due to their excellent properties.[1-5] In particular, CQDs have been widely used as prospective emissive materials for next-generation displays due to their many advantages, such as band gap tuning across the full color spectrum and high quantum efficiency.[6-8] However, the highly toxic and hazardous nature of Cd-based CQDs severely restricts their application to eco-friendly optoelectronic devices.[6] Therefore, further developments are required for novel CQDs, such as Cd-free CQDs, which have outstanding opto-electrical properties that are comparable to the well-known CdSe CQDs.

The group III-V CQDs, especially InP, are considered the next generation of CQDs with broad band-gap controllability.[7] However, despite the superior characteristics, III-V CQDs have drawbacks regarding low quantum yield (QY) as well as low stabilities. The use of metal nitride semiconductors has been suggested as an alternative solution to solve the problems raised in the group III-V CQDs mentioned above. GaN and $In_xGa_{1-x}N$ are commercially utilized as ultraviolet (UV) and green light emitting diodes (LEDs);[8] they exhibit superior chemical stabilities, high carrier mobilities, high light absorption coefficients and low toxicities.[12] Notably, the band gap of $In_xGa_{1-x}N$ can theoretically be tuned from 0.7 eV to 3.4 eV[9] by altering the Ga and In metal fractions. Due to ease of controllability of the band gap as well as excellent electrical properties of $In_xGa_{1-x}N$, many studies have been conducted to realize various emission colors for LED applications[10] through the control of the In and Ga ratio.

However, in contrast to theoretical expectations, achieving color control, especially for red emission, has proven to be nearly impossible due to the poor stability of the $In_xGa_{1-x}N$ for the In-rich alloy states when using the chemical vapor deposition (CVD) process. This instability originates from the intrinsic

differences in Ga and In, which are attributed to covalent radii divergence, lattice mismatch, and vapor pressure differences.[11,12] Only green emission from $In_xGa_{1-x}N$ was achieved for the low-temperature CVD process (~300-400 °C), but its optical property was still poor due to the low crystallinity. In addition, growth of $In_xGa_{1-x}N$ using a CVD process is not desirable for flexible device applications.

To solve these critical drawbacks, solution-based synthetic routes have been suggested as alternative methods. However, in most cases, metal nitrides synthesized using wet-chemical methods were largely composed of pure GaN or an extremely low In fraction.[13-17] As a result, realization of green and red emission for metal nitride CQDs has not been reported to date. Furthermore, the reports of metal nitride nanoparticles in the literature indicated low luminescence efficiency as well as a broad full width at half maximum (FWHM).

In this article, we report the synthesis of green to blue emissive $In_xGa_{1-x}N$ CQDs by using a hot-injection method and demonstrate the QLEDs using these CQDs for the first time. By varying the metal composition (In and Ga ratio) and size control (i.e., the quantum confinement effect)[18], band-gap tuned $In_xGa_{1-x}N$ CQDs were successfully synthesized. QLEDs fabricated using these CQDs exhibit green electroluminescence (EL) originating from the $In_xGa_{1-x}N$ CQDs. Our results demonstrate that $In_xGa_{1-x}N$ CQDs are a promising alternative to conventional CQDs containing Cd, thereby enabling eco-friendly displays.

## Results and Discussion

Fig. 1 (a) and (b) shows the X-ray diffraction (XRD) pattern of $In_xGa_{1-x}N$ CQDs of different metal compositions. From the XRD results, the GaN CQDs are determined to be in the cubic phase with (111), (220), and (311) planes, and the InN CQDs are in the cubic phase with (111), (200), (220), (311), and (400) planes. To verify the alloy states of the $In_xGa_{1-x}N$ CQDs, the changes in the peak position according to the changes in the metal fractions were investigated. By increasing the In fraction in the GaN CQDs, the peaks related to the GaN planes were shifted to the lower 2q region, and the peaks related to the InN planes were newly observed. In addition, the peaks from GaN were broad, but the peaks related to InN were sharp and of high intensity, indicating that the InN phases have higher crystallinities than those of the GaN phases. These results were atypical because high-quality InN crystals are more difficult to grow than GaN crystals.[31] Generally, the quality of the metal nitrides is strongly affected by substrate and growth temperature.[19,31] In particular, the extremely low decomposition temperature of InN makes it impossible to increase the growth temperature to achieve high crystallinity. As a result, high-quality InN or In-rich $In_xGa_{1-x}N$ are more difficult to grow than GaN or Ga-rich $In_xGa_{1-x}N$.[20,21] Therefore, the XRD results strongly suggest that it is possible to grow high quality In-rich $In_xGa_{1-x}N$ using our wet-chemical synthetic procedure. To identify the metal composition of $In_xGa_{1-x}N$ CQDs in detail, inductively coupled plasma mass spectroscopy (ICP-MS) analysis was conducted; details of the analysis results are described in Fig. S1 (a) in the supporting information.

The chemical states of the $In_xGa_{1-x}N$ CQDs were examined by X-ray photoelectron spectroscopy (XPS). Fig. 1 (c) and (d) show the binding states of the $In_xGa_{1-x}N$ CQDs at the $Ga3d_{5/2}$ and N1s spectral regions. The spectrum of $Ga3d_{5/2}$ consisted of two peaks, corresponding to the $Ga_2O_3$ and GaN binding states.[22] With increasing In metal fraction, the peak positions of both $Ga_2O_3$ and GaN shifted to lower energy states, and the peak intensity of $Ga_2O_3$ increased. The relative peak intensities of the $Ga_2O_3$ and GaN states were found to be strongly related to the Ga fractions in both the surface and the internal sites in $In_xGa_{1-x}N$ CQDs. The Ga atoms on the surface can be bonded to nitrogen (from metal nitride complexes) and/or oxygen (from oleic acid; O.A.). By increasing the In fraction, the oxygen binding states became more dominant than the nitrogen bonding states due to the decrease in the Ga-N binding ratio at the internal sites. The N1s spectra in Fig. 1 (d) revealed the metal to nitrogen binding states. A high In fraction induced a shift in the binding energy of the N1s state to a lower energy state due to the change in the lattice environment resulting from the electronegativity change of $In_xGa_{1-x}N$ CQDs. These results provide direct evidence that the $In_xGa_{1-x}N$ CQDs exhibited the metal-N binding alloy state with well-distributed Ga and In conditions. The In3d binding results are shown in Fig. S1(b). From the X-ray characterization results in Fig. 1, the crystal structures and the binding energy of $In_xGa_{1-x}N$ CQDs in the alloy state were well demonstrated.

Fig. 2 shows the Ultraviolet-visible (UV-vis) absorption and the photoluminescence (PL) spectra of $In_xGa_{1-x}N$ CQDs according to the metal composition. The figures show the effects of the metal fraction on the optical properties of the $In_xGa_{1-x}N$ CQDs. No significant changes in the $1^{st}$ excitonic peak (~520 nm) were observed in the UV-Vis absorbance; only a slight broadening of the peak was observed as the In fraction increased. Fig. 2(b) shows the PL spectra of $In_xGa_{1-x}N$ CQDs for different metal compositions. In contrast to theoretical expectations, no PL spectral shift was observed with variation of the In fraction, and all the $In_xGa_{1-x}N$ CQDs exhibit similar PL spectra with dominant green emission. The reasons for no PL spectra change according to the metal fraction will be explained in Fig. 3.

The PL spectra of $In_xGa_{1-x}N$ CQDs consisted of three peaks at ~460, ~520 and ~560 nm. From Fig. 2 (c), two peaks at ~460 and ~520 nm were confirmed to be related to GaN. Generally, high-quality GaN exhibits PL emission in the UV region (365 and 375 nm), and GaN with lattice defects and/or oxygen doping[23] exhibit greenish yellow PL emission.[13,24] Therefore, GaN and $In_xGa_{1-x}N$ CQDs synthesized via the hot-injection method are confirmed to have relatively high numbers of defect states due to low crystallinity and oxygen binding with O.A. The $In_xGa_{1-x}N$ CQDs exhibit broader PL spectra than those of the GaN CQDs due to the contribution of PL emission at ~560 nm (Fig. 2 (b) and (c)). The origin of the shoulder peak (~560 nm) will also be explained in Fig. 3 in detail. With increasing In metal fraction, the PL intensity of $In_xGa_{1-x}N$ CQDs was observed to decrease and the relative PL intensity ratio for emission at ~460 nm vs. emission at 520 nm was observed to increase due to the rapid decrease of the PL intensity at ~520 nm. The relative PL-QY of the $In_xGa_{1-x}N$ CQDs according to the metal fraction variation is shown in Fig. S2, which well matched the PL intensity change shown in Fig. 2 (b).

The optical properties of the CQDs can be varied via size control under the same metal composition. From the UV-vis absorption and the PL spectra of the $In_{0.25}Ga_{0.75}N$ CQDs of different size (Fig. S3), the band gap of $In_xGa_{1-x}N$ CQDs was found to be well controlled via the quantum confinement effect. Fig. S4 and Fig. S5 show the PL maximum peak shift and the transmission electron microscope (TEM) images of $In_{0.25}Ga_{0.75}N$ CQDs for different O.A. concentrations, respectively. From the TEM results, the variations in the optical properties of the $In_{0.25}Ga_{0.75}N$ CQDs were confirmed to be due to the quantum confinement effect.

To investigate the origin of each of the peaks as well as the cause of the lack of PL spectral shift in $In_xGa_{1-x}N$ CQDs (x = 0 to 0.75), we conducted temperature-dependent PL (T-PL) experiments, as shown in Fig. 3. The GaN CQDs exhibit two peaks at ~460 and ~520 nm at all temperatures (Fig. 3 (a)). However, the relative PL intensities of the GaN CQDs at ~460 and at 520 nm were observed to change with the temperature. With increasing temperature, the reduction of the PL intensity at ~460 nm was much faster than that at ~520 nm. The radiative PL emission at ~460 nm has been suggested to be more influenced by defects related to non-radiative recombination than the PL emission at ~520 nm. This non-radiative quenching originates from lattice vibrational energy loss due to the low crystallinity of GaN.[23]

The $In_xGa_{1-x}N$ CQDs (x = 0.25 to 0.75) also exhibit variations in PL intensity with temperature. Fig. 3 (b) shows T-PL spectra of $In_{0.25}Ga_{0.75}N$ CQDs (low concentration of In). As was the case for the GaN CQDs, the PL intensities at ~460 and, in particular, ~520 nm also changed with temperature due to defects. Importantly, new PL peaks at ~560 and ~580 nm, which originated from the In alloy-mediated states, were observed at low temperature. The PL intensity at ~520 nm decreased at a slightly higher rate than that at ~560 nm with increasing temperature. This result indicated that the GaN mediated state was more governed by non-radiative recombination than In alloy-mediated state.

Fig. 3 (c) shows T-PL spectra of $In_{0.5}Ga_{0.5}N$ CQDs (same concentration of Ga and In). When the In fraction increased, the PL intensities at ~560 and ~580 nm significantly increased compared with those of the $In_xGa_{1-x}N$ CQDs with low In fractions. From this result, the PL emissions at ~560 and ~580 nm were confirmed to directly originate from the In alloy states. Reduction of the PL intensity at ~560 nm in $In_{0.5}Ga_{0.5}N$ CQDs is slightly faster than that at ~520 nm, in contrast to the trend shown in the $In_xGa_{1-x}N$ CQDs with a low In fraction. This result suggested that the contribution of the In alloy-mediated state increased with increasing In fraction and that the radiative recombination states in $In_{0.5}Ga_{0.5}N$ CQDs were affected by both the GaN and In alloy-mediated states; however, the radiative recombination was influenced slightly more by the In alloy-mediated states.

Based on trend of the PL spectra change according to the In metal fraction, the PL emission at ~560 and ~580 nm should significantly increase in $In_{0.75}Ga_{0.25}N$ CQDs (high In fraction). However, interestingly, the $In_{0.75}Ga_{0.25}N$ CQDs exhibited different PL spectra compared with those of the $In_xGa_{1-x}N$ CQDs (x=0 to 0.5); these differences are highlighted by the following observations: (1) The PL peaks at ~560 and ~580

nm are not clearly observed. (2) The PL peak at ~520 nm red-shifts with increasing temperature. (3) PL intensity at ~460 nm is significantly high. (4) A new PL emission at ~490 nm is observed. When the In metal fraction is larger than 75 %, the number of In-mediated states with higher defect levels also dramatically increased (the PL-QY decreased from 34 % to 3 % in Fig. S2). As a result, the PL properties of $In_{0.75}Ga_{0.25}N$ were found to be strongly affected by the In alloy-mediated states. Therefore, the PL emissions at ~560 and ~580 nm were strongly quenched and not observable, even at low temperatures. The red-shift of the PL peak at ~520 nm was caused by exciton-phonon interactions,[25] which resulted from the defect-sensitive condition due to the increase in the In fraction.

In Fig. 3(b)-(d), the PL intensity at ~460 nm in $In_xGa_{1-x}N$ CQDs was observed to increase with increasing In fraction. These phenomena can be explained by the relative PL quenching rates of the GaN-mediated peak (~460 nm) and In alloy-mediated peaks (~560 and ~580 nm). When the In fraction increased, the PL intensity of the $In_xGa_{1-x}N$ CQDs decreased due to the increase in the number of defect states. The In alloy-mediated PL emission was found to be more sensitive to defects and more easily quenched than that related to the GaN-mediated states. Therefore, the PL intensities at ~560 and ~580 nm were reduced compared to that of the PL intensity at ~460 nm in the $In_xGa_{1-x}N$ CQDs, i.e., the PL intensity at ~460 nm appears to be high in the $In_xGa_{1-x}N$ CQDs. The T-PL experiments on $In_xGa_{1-x}N$ CQDs demonstrated not only large and rapid PL quenching but also the emergence of red-shifted energy levels induced by the In-metal alloy. The power-dependence and time-correlated single photon counting (TCSPC) results of $In_xGa_{1-x}N$ CQDs are shown in Fig. S6 and Fig. S7.

From Fig. 2 and Fig. 3, the PL spectra of $In_xGa_{1-x}N$ CQDs consisted of multiple peaks, with each of the peak intensities and ratios changing by varying the metal fraction. As mentioned above, the optical properties of $In_xGa_{1-x}N$ CQDs were determined by their phase conditions. Unfortunately, the XRD results in Fig. 1 do not clearly show the phase information for the $In_xGa_{1-x}N$ CQDs due to the low crystallinity; therefore, other technical methods must be utilized to determine the relationship between the optical properties and the phase condition of the $In_xGa_{1-x}N$ CQDs. As shown in the results of A. Rizzi *et al.*[26], the crystal states of the $In_xGa_{1-x}N$ CQDs consisted of multiple phase states, and their crystal states were controlled by the phase differences. To investigate the phase states of $In_xGa_{1-x}N$ CQDs, X-ray absorption spectroscopy (XAS) studies were conducted, which consisted of the X-ray absorption near edge spectrum (XANES, Fig. S8) and the X-ray absorption fine structure (XAFS, Fig. 4). All of the characterizations were conducted in the In K-edge state. Fig. 4 (a) shows a magnified view of the XAFS results of the $In_xGa_{1-x}N$ CQDs (x = 0.25 to 1), which demonstrates each phase of the $In_xGa_{1-x}N$ CQDs. All the $In_xGa_{1-x}N$ CQDs exhibit three peaks in the 2.2 to 3.4 Å range. For convenience, the three regions representing these peaks were denoted A, B, and C. The coordination peaks in the A and B regions were located between the In-N and In-In coordination bindings, and the C region was located near the In-In coordination site. This XAFS results indicated that the crystal conditions of our $In_xGa_{1-x}N$ CQDs consisted of multiple phase states. Fig. 4 (b) shows the change in the Fourier transform intensity of the A, B, and C regions with the change in the In fraction. With increasing In fraction, the Fourier transform

intensity of the A region decreased, that of the B region slightly increased, and that of the C region dramatically increased, i.e., each phase had a specific metal ratio, but the inherent phases did not change due to the change in the metal fraction. The multiple phase generation and Fourier transform intensity change with metal fraction variation suggested that $In_xGa_{1-x}N$ CQDs had multiple energy states originating from multiple phases, which results in multiple peaks in the PL spectrum. The XANES and wide-range XAFS results are described in Fig. S8 (a) and Fig. S8 (b), respectively.

Using the resulting $In_xGa_{1-x}N$ CQDs, QLEDs were fabricated, and the device performances of the QLEDs were characterized (Fig. 5). The fabricated QLEDs had a simple structure of ITO/ZnO (40 nm)/$In_xGa_{1-x}N$ CQDs (10 nm)/Hole injection layers (HILs) (60-80 nm)/$MoO_3$ (10 nm)/Ag (100 nm). $In_{0.25}Ga_{0.75}N$ CQDs were used as the emissive materials layer because they exhibited the highest PL-QY. The energy levels of the highest occupied molecular orbital (HOMO) and the lowest unoccupied molecular orbital (LUMO) of the $In_{0.25}Ga_{0.75}N$ CQDs were determined from ultraviolet photoemission spectroscopy (UPS, Fig. S9) and the optical band gap, which was estimated from the absorption and PL results. As shown in Fig. 5 (a), $In_{0.25}Ga_{0.75}N$ CQDs have a deep HOMO level compared to other CQDs (such as CdSe and InP) or general luminescent materials. The deep HOMO energy level of $In_xGa_{1-x}N$ CQDs induced high charge (especially hole) injection barriers; therefore, an inverted structure and several hole transport layers (HTLs) were used to reduce the charge injection barriers. Chemically synthesized ZnO NPs were used to form the electron injection layer (EIL). Layers of 4,4'-Bis(*N*-carbazolyl)-1,1'-biphenyl (CBP)[27], 1,3,5-tris(N-phenylbenzimidazol-2-yl)benzene (TPBi)/CBP, and CBP/ 1,4,5,8,9,11-hexaazatriphenylene-hexacarbonitrile (HAT-CN)[28] were used as HILs, and the devices with these different HILs were denoted as devices A, B, and C, respectively.

Fig. 5 (b) and Fig. 5 (c) show the current and luminance vs. voltage curves of the QLEDs, respectively. Device A and device B exhibit similar current and luminance characteristics. The slightly higher turn-on of device B compared to device A is due to the thicker HTL thickness. However, device C exhibits a lower current as well as a luminance with a high turn-on voltage. This poor performance of device C indicates that the charge balance in device C is poor when CBP/HAT-CN was used as the HIL, in contrast to the previous results.[29] The maximum luminance of ~45 cd/$m^2$ was measured at 18 V in the device B. The TPBi layer improved the charge balance by accumulation of holes at the interface between TPBi and CBP.[28] The power efficiency vs. luminance curve of device B was described in Fig. S10 (a).

Fig. 5 (d) shows the EL spectrum of device B at 18 V. The shape and peak position in the EL spectrum were the same as those of the PL spectrum. Therefore, the EL spectrum of the QLED is confirmed to originate from the $In_{0.25}Ga_{0.75}N$ CQDs. The EL spectrum of the QLED did not change with applied voltage, as shown in Fig. S10 (b), which indicates that $In_{0.25}Ga_{0.75}N$ CQDs have high electrical and thermal stabilities. The EL emission at ~410 nm at high applied voltage might originate from CBP.

To verify the potential of our $In_xGa_{1-x}N$ CQDs for use in flexible LEDs, a QLED with an ITO-coated PET as an electrode was fabricated and characterized. Fig. 5 (e) presents a digital camera image of green EL

emission from the QLED. This result indicates that $In_xGa_{1-x}N$ CQDs synthesized using the wet-chemical method can be a good candidate for replacing conventional CQDs with cadmium in various optoelectronic applications, especially eco-friendly flexible displays.

## Conclusion

Green emissive $In_xGa_{1-x}N$ CQDs were synthesized via a wet-chemical synthetic method, and flexible QLEDs using these CQDs were demonstrated for the first time. The band gaps of the $In_xGa_{1-x}N$ CQDs were varied by varying the metal fraction and by particle size control. Green and blue emissive $In_xGa_{1-x}N$ CQDs were easily realized via particle size control. However, in contrast to theoretical expectations, varying the metal fraction was not effective for tuning the band gap of $In_xGa_{1-x}N$ CQDs. From T-PL experiments of the $In_xGa_{1-x}N$ CQDs, the PL emissions at ~560 and ~580 nm were found to originate from the In-mediated states, demonstrating the possibility of band gap tuning from the red emission of $In_xGa_{1-x}N$ CQDs at low temperature. The XAFS (XANES) results demonstrated that the crystal structures of $In_xGa_{1-x}N$ CQDs consist of multiple-phase states and that each phase ratio changed with the metal fraction. In addition, the multiple peaks in the PL spectra of $In_xGa_{1-x}N$ CQDs resulted from the multiple phases, which have multiple energy states. Inverted structured QLEDs were fabricated based on the $In_xGa_{1-x}N$ CQDs, and the device performances were characterized. The QLEDs exhibited green EL emission with a maximum luminance of ~45 $cd/m^2$. Although further improvements in device performance are required, this work represents a demonstration of green QLEDs using chemically synthesized $In_xGa_{1-x}N$ CQDs as the emissive material.

## Experimental Methods

Synthesis of InxGa1-xN CQDs: Unless noted otherwise, all synthetic steps were performed under purified argon atmosphere using a M. Braun glovebox or standard Schlenk line techniques. The indium-gallium oleate complex solution was prepared by mixing x (0 to 1) mmol of indium(III) acetylacetonate, 1-x mmol of gallium(III) acetylacetonate, 4.525 mL of 1-octadecene (ODE), and 0.6 to 2.2 mmol of oleic acid under vigorous mixing by increasing the temperature to 300 °C. When the solution temperature reached 300 °C, a mixture of 0.9 mL of ODE and 0.5 mmol of hexamethyldisilazane (HMDS) was rapidly injected into the reactor. The solution was maintained at 300 °C for 0.5 h and then cooled to room temperature to terminate the reaction. For purification of the InxGa1-xN CQDs, a precipitation/re-dispersion method was used. The product solution was precipitated with excess anti-solvent and then re-dispersed in hexane. After repeating the purification procedure (typically 5 times), the precipitated CQDs were dried under an argon flow for 5 min and then dispersed in various organic solvents (approximately 50 mg mL-1). Characterization of the InxGa1-xN CQDs: Characterization of the morphology, crystal structure, binding energy, and composition of the metal nitride CQDs were investigated via high-resolution transmission electron microscopy (TEM, JEOL, JEM-2100F), X-ray diffraction (XRD, Rigaku, D/MAZX 2500V/PC, Cu-Kα radiation source, λ = 0.15418 nm), X-ray photoelectron spectroscopy (XPS, Escalab 250xi), inductively

coupled plasma-mass spectroscopy (ICP-MS, Perkin Elmer, Elan DRC-II), and X-ray absorption spectroscopy (XAS and XANES, Pohang Accelerator Lab, XAFS 7D line). Ultraviolet photoelectron spectroscopy (UPS, Escalab 250xi), UV-visible spectroscopy (UV-Vis, Agilent), room temperature solution PL (Agilent), temperature- and power-dependent film PL, and time-correlated single photon counting (TCSPC) were utilized to characterize the optical properties of the metal nitride CQDs. Temperature and power dependent PL experiments: PL spectra were measured using a 15-cm monochromator (SP-2150i, Acton) equipped with a photomultiplier tube (PMT) and using a tunable Ti:sapphire laser (Mira900, Coherent) as the excitation light source. The temperature was varied between 20 K and 300 K using a He closed-cycle Displex refrigeration system. The excitation laser power at 375 nm was changed from 0.28 to 11.6 mW. Time-Correlated Single Photon Counting (TCSPC) Experiments: The PL decays of the InxGa1-xN CQDs were investigated using time-correlated single photon counting (TCSPC) measurements. The second harmonic (SHG = 375 nm) of a tunable Ti:sapphire laser (Mira900, Coherent), with a ∼150 fs pulse width and 76 MHz repetition rate, was used as the excitation source. The PL emission was spectrally resolved using some collection optics and a monochromator (SP-2150i, Acton). A TCSPC module (PicoHarp, PicoQuant) with a MCP-PMT (R3809U-59, Hamamatsu) was used for ultrafast measurement of the PL decay. The total instrument response function (IRF) for the PL decay was less than 140 ps, and the temporal resolution was less than 10 ps. The deconvolution of the actual fluorescence decay and the IRF was performed using fitting software (FlouFit, PicoQuant) to determine the time constant associated with each of the observed exponential decays. Characterization of the Valence band (HOMO) and the Conduction band (LUMO) of In0.25Ga0.75N CQDs: The energy levels of the In0.25Ga0.75N CQDs were measured in the film state; the CQD films were spin coated onto ZnO-NP-coated ITO substrates. A gold-coated ITO substrate was used as a reference. The HOMO energy level was determined from the incident photon energy (21.2 eV), the high binding energy cut-off (Ecutoff), and the onset point in the valence band state (Eonset) according to the equation. The LUMO energy level was determined by using the HOMO energy level and the band gap of the In0.25Ga0.75N CQDs estimated from the absorption and PL results. Device fabrication and characterization: The fabricated QLEDs had a structure of ITO/ZnO (40 nm)/In0.25Ga0.75N CQDs (10 nm)/HTL (60-80 nm)/MoO3 (10 nm)/Ag (100 nm). The ITO substrates were cleaned with organic solvents and O2 plasma treatment for 10 min. The electron injection ZnO nanoparticle (NP) films with thicknesses of 40 nm were spin-coated on the ITO substrates using 45 mg/mL of the ZnO NPs solution (in butanol) and then dried at 150 °C for 30 min. An In0.25Ga0.75N CQDs layer with a thickness of 10 nm was spin-coated onto the ZnO-NP layer using a 7.5 mg/mL CQDs solution (in octane); the CQDs layer was used as the emitting layer. Three different hole injection layers, CBP (60 nm), TPBi (5 nm), and HAT-CN (20 nm), were thermally evaporated at a deposition rate of 1 ~1.5 Å s-1. A 10-nm-thick MoOx layer and a 100-nm-thick Ag layer were thermally evaporated on top of the hole injection layers as the cathode. A PET-ITO substrate (Sigma-Aldrich, 60 ohm cm-2) replaced the glass ITO substrate for fabrication of the flexible QLED. The current-voltage-luminance characteristics of the QLEDs were measured using a Keithley 2400 source measurement unit and a luminance meter (Minolta, CS-100A). The EL spectra were measured using a Fiber Optic Spectrometer. (K-MAC, SV 2100).

# Declarations

Acknowledgements

J.P. would like to thank the New & Renewable Energy Core Technology Program of the Korean Institute of Energy Technology Evaluation and Planning (KETEP) for the financial support, granted from the Ministry of Trade, Industry & Energy, Republic of Korea (No. 20133030000180). The experiments at the PLS were partially supported by PAL at POSTECH. C.L.L. would like to thank the Basic Science Research Program through the Ministry of Education (NRF-2013R1A1A2006742) and the APRI research program, granted from Gwangju Institute of Science and Technology for the financial support.

Author contributions

J.P. and Y.H.S. conceived the idea. Y.J and Y.H.S designed and performed the main experiments. J.P., Y.H.S., and Y.J. prepared the manuscript. J.P. supervised the project. All the authors discussed the results and contributed to the manuscript.

# References

1. Murray, C. B., Norris, D. J. & Bawendi, M. G. Synthesis and characterization of nearly monodisperse CdE (E = sulfur, selenium, tellurium) semiconductor nanocrystallites. *J. Am. Chem. Soc.* 115, 8706-8715 (1993).
2. Bawendi, M. G., Steigerwald, M. L. & Brus, L. E. The Quantum mechanics of larger semiconductor clusters ("Quantum Dots"). *Annu. Rev. Phys. Chem.* 41, 477-496 (1990).
3. Alivisatos, A. P. Perspectives on the physical chemistry of semiconductor nanocrystals. *J. Phys. Chem.* 100, 13226-13239 (1996).
4. Singh, A. *et al.* Compositionally tunable photoluminescence emission in Cu2 ZnSn(S1-x Sex )4 Nanocrystals. *Angew. Chem. Int. Ed.* 52, 9120-9124 (2013).
5. Zou, Y., Su, X. & Jiang, J. Phase-controlled synthesis of Cu2ZnSnS4 nanocrystals: the role of reactivity between Zn and S. *J. Am. Chem. Soc.* 135, 18377-18384 (2013).
6. Hardman, R. A Toxicologic review of quantum dots: toxicity depends on physicochemical and environmental factors. *Environ. Health Persp.* 114, 165-172 (2006).
7. Yang, X. *et al.* Full visible range covering InP/ZnS nanocrystals with high photometric performance and their application to white quantum dot light-emitting diodes. *Adv. Mater.* 24, 4180-4185 (2012).
8. Nakamura, S. InGaN-based blue/green LEDs and laser diodes. *Adv. Mater.* 8, 689-692 (1996).
9. Millot, M., Geballe, Z. M., Yu, K. M., Walukiewicz, W. & Jeanloz, R. Red-green luminescence in indium gallium nitride alloys investigated by high pressure optical spectroscopy. *Appl. Phys. Lett.* 100, 162103 (2012).
10. Hahn, C. *et al.* Epitaxial growth of InGaN nanowire arrays for light emitting diodes. *ACS Nano* 5, 3970-3976 (2011).

11. Keller, S. *et al.* Growth and characterization of bulk InGaN films and quantum wells. *Appl. Phys. Lett.* 68, 3147-3149 (1996).
12. Strite, S. & Morkoç, H. GaN, AlN, and InN: A review. *J. Vac. Science & Tech. B* 10, 1237-1266 (1992).
13. Pan, G., Kordesch, M. E. & Van Patten, P. G. New pyrolysis route to GaN quantum dots. *Chem. Mat.* 18, 3915-3917 (2006).
14. Sardar, K. & Rao, C. N. R. New solvothermal routes for GaN nanocrystals. *Adv. Mater.* 16, 425-429 (2004).
15. Sun, X. & Li, Y. $Ga_2O_3$ and GaN semiconductor hollow spheres. *Angew. Chem. Int. Ed.* 43, 3827-3831 (2004).
16. Chen, Z. *et al.* Large-scale cubic InN nanocrystals by a combined solution- and vapor-phase method under silica confinement. *J. Am. Chem. Soc.* 134, 780-783 (2012).
17. Bhaviripudi, S., Qi, J., Hu, E. L. & Belcher, A. M. Synthesis, characterization, and optical properties of ordered arrays of III-Nitride Nanocrystals. *Nano lett.* 7, 3512-3517 (2007).
18. Murray, C. B., Kagan, C. R. & Bawendi, M. G. Synthesis and characterization of monodisperse nanocrystals and close-packed nanocrystals assemblies. *Ann. Rev. Mat. Sci.* 30, 545-610 (2000).
19. Strite, S. *et al.* Structural properties of InN films grown on GaAs substrates: observation of the zincblende polytype. *J. Crystal Growth* 127, 204-208 (1993).
20. Pantha, B. N., Li, J., Lin, J. Y. & Jiang, H. X. Evolution of phase separation in In-rich InGaN alloys. *Appl. Phys. Let.* 96, 232105 (2010).
21. Kim, H. J. *et al.* Compositional analysis of In-rich InGaN layers grown on GaN templates by metalorganic chemical vapor deposition. *J. Crystal Growth* 310, 3004-3008 (2008).
22. Carin, R., Deville, J. P. & Werckmann, J. An XPS study of GaN thin films on GaAs. *Surf. Interface Anal.* 16, 65-69 (1990).
23. Reshchikov, M. A. & Morkoç, H. Luminescence properties of defects in GaN. *J. Appl. Phys.* 97, 061301 (2005).
24. Coffer, J. L., Johnson, M. A., Zhang, L., Wells, R. L. & Janik, J. F. Influence of precursor route on the photoluminescence of bulk nanocrystalline gallium nitride. *Chem. Mater.* 9, 2671-2673 (1997).
25. Yeo, I., Dong Song, J. & Lee, J. Temperature-dependent energy band gap variation in self-organized InAs quantum dots. *Appl Phys. Let.* 99, 151909 (2011).
26. Segura-Ruiz, J., Martínez-Criado, G., Denker, C., Malindretos, J. & Rizzi, A. Phase separation in single InxGa1–xN nanowires revealed through a gard X-ray synchrotron nanoprobe. *Nano lett.* 14, 1300-1305 (2014).
27. Bae, W. K. *et al.* R/G/B/natural white light thin colloidal quantum dot-based light-emitting devices. *Adv. Mater.* 26, 6387-6393 (2014).
28. Ji, W. *et al.* Efficient quantum dot light-emitting diodes by controlling the carrier accumulation and exciton formation. *ACS appl mater. Inter.* 6, 14001-14007 (2014).

29. Kim, Y.-K., Won Kim, J. & Park, Y. Energy level alignment at a charge generation interface between 4,4[sup ]-bis(N-phenyl-1-naphthylamino)biphenyl and 1,4,5,8,9,11-hexaazatriphenylene-hexacarbonitrile. *Appl. Phys. Lett.* 94, 063305 (2009).
30. Bhat, T. N. *et al.* Evidences for ambient oxidation of indium nitride quantum dots. *phys. status solidi (b)* 248, 2853-2856 (2011).
31. Gil, B. *et al*. *Group III nitride semiconductor compounds physics and applications Ch.2* (Clarendon press, Oxford, 1998)

# Figures

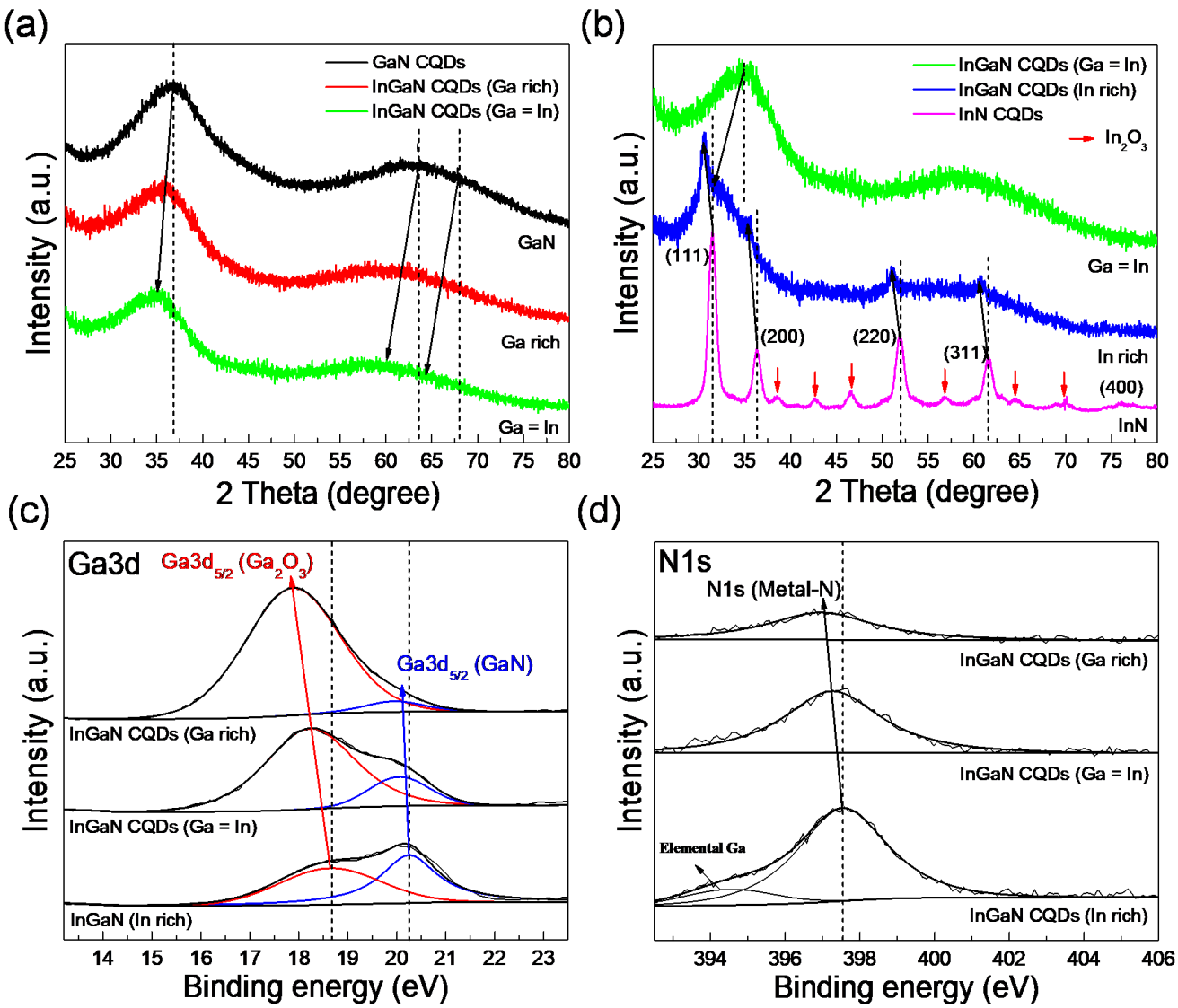



**Figure 1**

X-ray characterization of $In_xGa_{1-x}N$ CQDs. (a) XRD spectra of $In_xGa_{1-x}N$ CQDs (x = 0, 0.25, and 0.5) and (b) $In_xGa_{1-x}N$ CQDs (x = 0.5, 0.75, and 1) [GaN PDF number: 00-050-0792, and InN PDF number: 01-088-

2365]. (A small amount of the $In_2O_3$ phase (red arrows) is attributed to the oxidation of InN CQDs due to air exposure during washing or the XRD measurement. [30]) XPS spectra of (c) Ga3d binding, and (d) N1s binding position of $In_xGa_{1-x}N$ (x = 0.25, 0.5, and 0.75). The XPS results were calibrated to the C1s peak (284.8 eV).

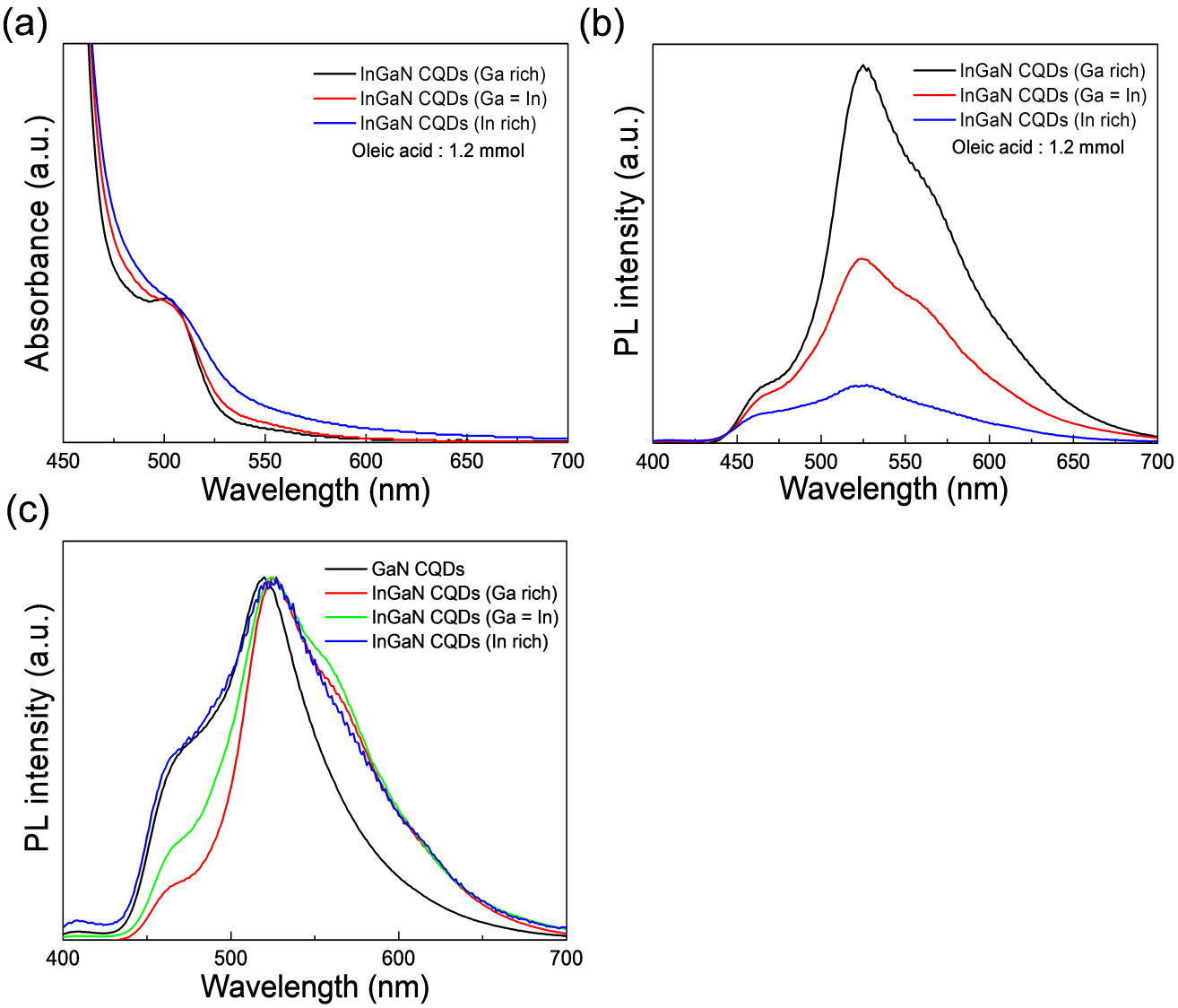



**Figure 2**

Band gap tuning of $In_xGa_{1-x}N$ CQDs via Ga- and In-metal composition variation. (a) UV-vis absorption and (b) PL spectra of $In_xGa_{1-x}N$ (x = 0.25, 0.5, and 0.75). (c) Normalized PL spectra of $In_xGa_{1-x}N$ (x = 0, 0.25, 0.5, and 0.75).

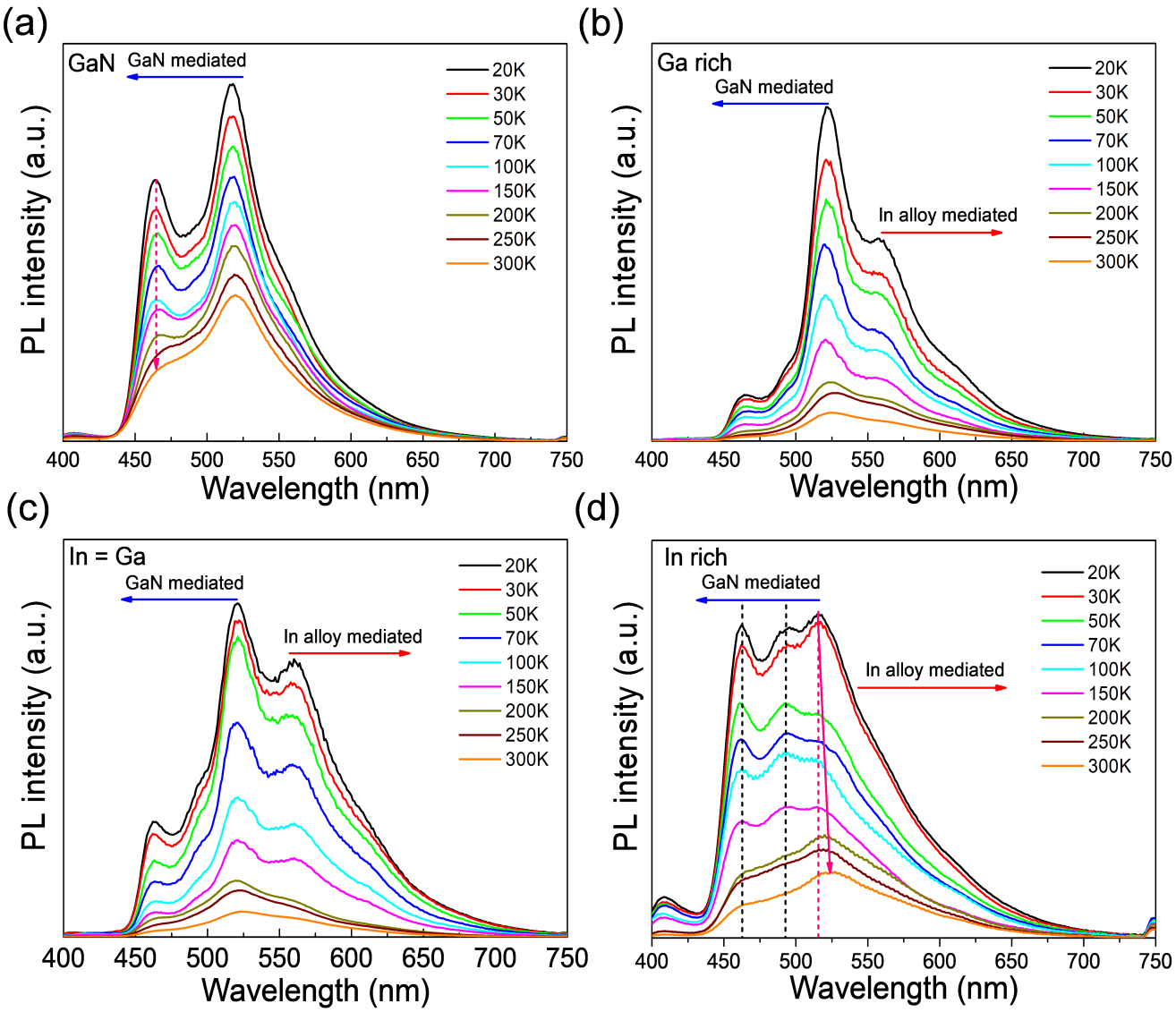



**Figure 3**

Temperature-dependent PL spectra of $In_xGa_{1-x}N$ CQDs. (a) GaN, (b) $In_{0.25}Ga_{0.75}N$, (c) $In_{0.5}Ga_{0.5}N$, and (d) $In_{0.75}Ga_{0.25}N$ CQDs-coated Si substrates. The fs tunable Ti:sapphire laser (Mira900, Coherent) was used as an excitation source ($\lambda_{exc}$ = 375 nm, excitation laser power: 1.1 mW).

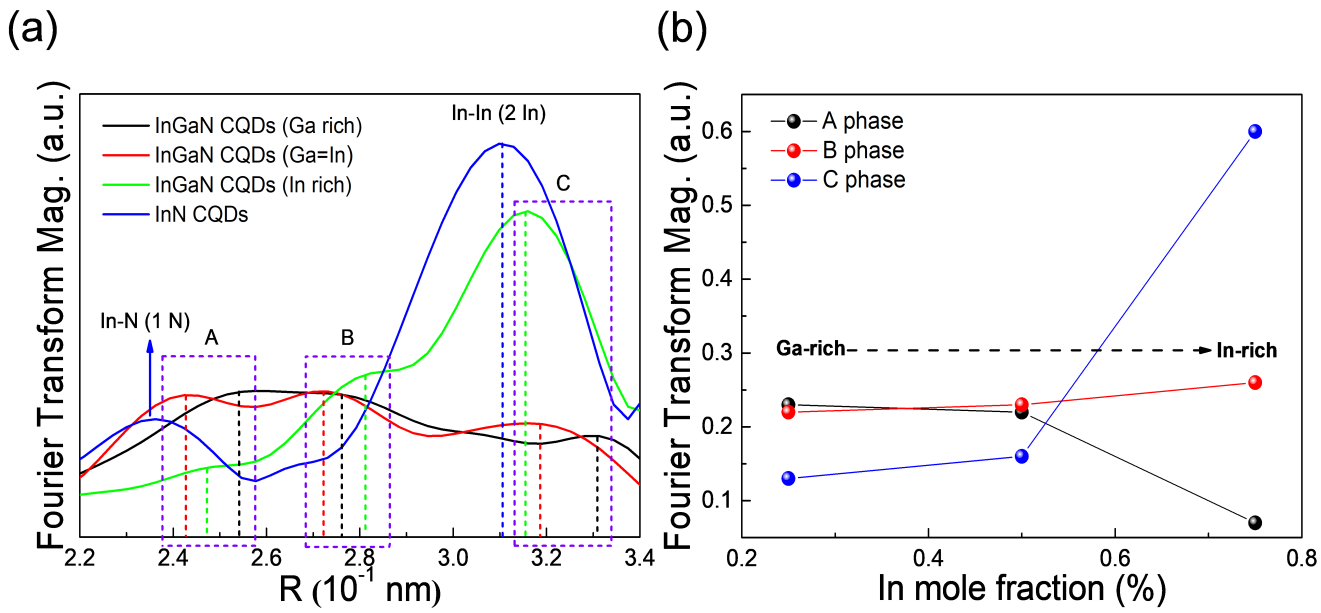



**Figure 4**

XAFS characterization of $In_xGa_{1-x}N$ CQDs. (a) XAFS spectra of $In_xGa_{1-x}N$ (x = 0.25, 0.5, 0.75, and 1). For comparison of the Fourier transform magnitude of each condition, the XAFS spectra were magnified in the range of 2.2 to 3.4 Å. (b) The Fourier transform magnitude of $In_xGa_{1-x}N$ (x = 0.25, 0.5, and 0.75) for the A, B, and C phases. The intensities were calibrated by using indium acetylacetonate as a reference.

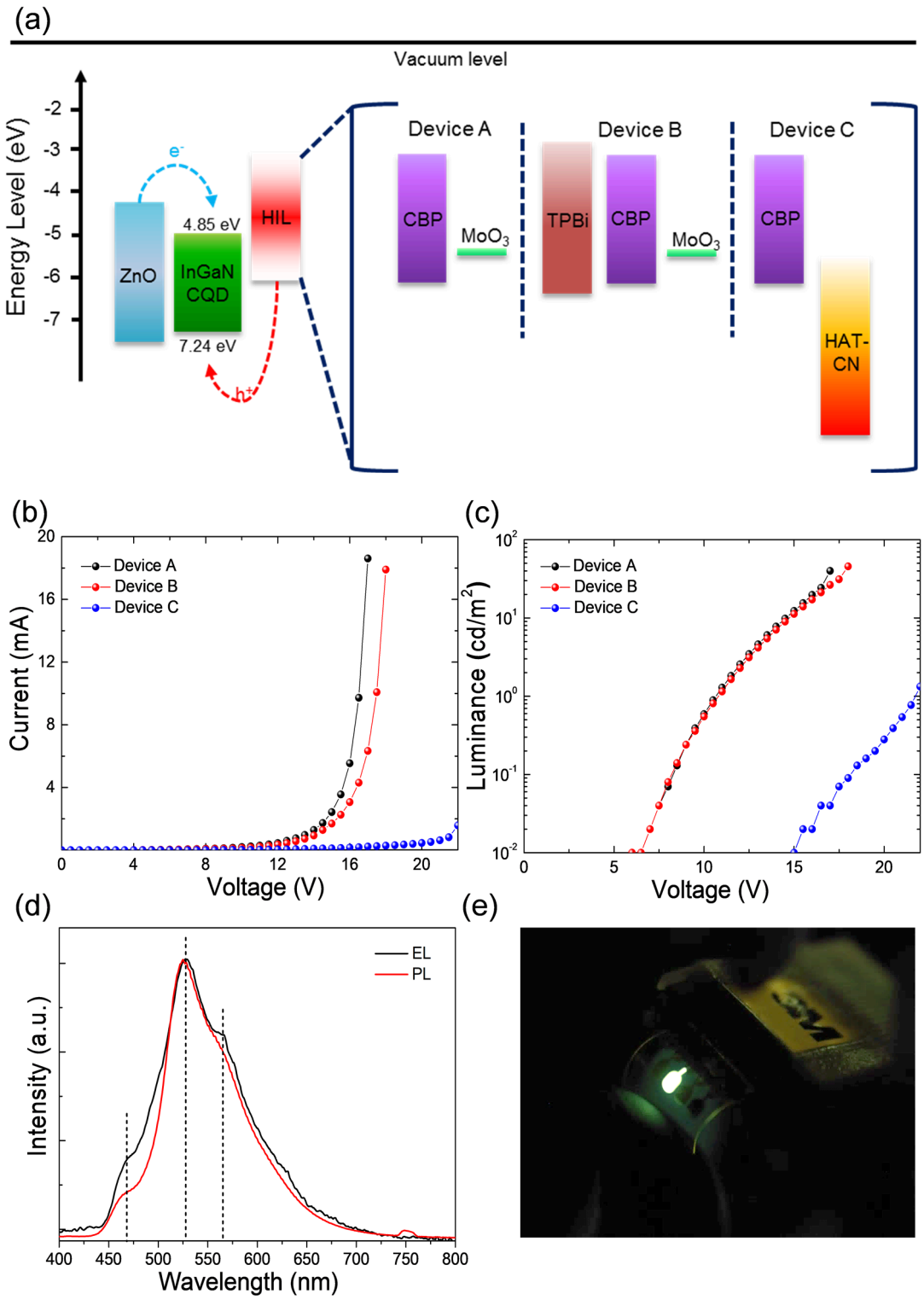



**Figure 5**

Device performance and characterization. (a) Schematic energy diagram of the QLEDs with different HILs. (b) Current vs. voltage, (c) luminance vs. voltage curves of the QLEDs with different HILs. (d) EL spectrum and (e) digital camera image of the QLED using $In_{0.25}Ga_{0.75}N$ CQDs as the emissive layer at 18 V.

## Supplementary Files

This is a list of supplementary files associated with this preprint. Click to download.

- SI.docx